Excerpt from the Proceedings of the 2011 COMSOL Conference in Boston

COMSOL-based Nuclear Reactor Kinetics Studies at the HFIR

David Chandler[*,1], James D. Freels[2], G. Ivan Maldonado[1], and R. T. Primm, III[3]
[1]University of Tennessee, Department of Nuclear Engineering
[2]Oak Ridge National Laboratory, Research Reactors Division
[3]Primm Consulting, LLC (ORNL, RRD retiree)
*Corresponding author: P. O. Box 2008, Oak Ridge, TN 37831-6399, chandlerd@ornl.gov

Abstract: The computational ability to accurately predict the dynamic behavior of a nuclear reactor core in response to reactivity-induced perturbations is needed to understand the behavior of existing reactors under "upset" conditions and to design the next generation of nuclear reactors. Space-time and point kinetics methodologies were developed for the purpose of studying the transient-induced behavior of the High Flux Isotope Reactor's (HFIR) compact core. The space-time simulations employed the three-energy-group neutron diffusion equations, and transients initiated by control cylinder and hydraulic tube rabbit ejections were studied.

The work presented here is the first step towards creating a comprehensive multiphysics methodology for studying the behavior of the HFIR core during transients (loss of off-site power, pump shutdown, reactivity perturbations, etc). The results of these studies show that point kinetics is adequate for small perturbations in which the power distribution is assumed to be time-independent, but space-time methods must be utilized to determine localized effects.

Keywords: HFIR, kinetics, neutronics.

1. Introduction

COMSOL was utilized to develop new space-time (ST) and point kinetics (PK) methodologies for the purpose of studying the transient-induced behavior of the High Flux Isotope Reactor (HFIR) core. The studies described herein are a continuation of those documented in Ref. 1.

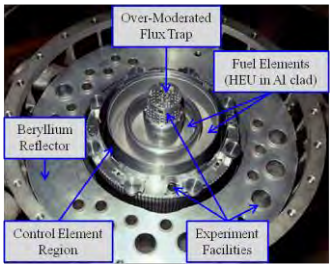

Figure 1. Mockup of the HFIR.

1.1 Brief Description of the HFIR

The HFIR is a versatile research reactor located at the Oak Ridge National Laboratory (ORNL). The steady-state neutron fluxes produced in this 85 MW_{th} reactor are utilized for cold and thermal neutron scattering, materials irradiation, isotope production, and neutron activation analysis. The HFIR is a pressurized, light water reactor that was designed with an over-moderated flux-trap (FT) and a large beryllium reflector in order to produce a large thermal flux-to-power ratio.

The central FT is surrounded by two concentric fuel annuli composed of involute-shaped fuel plates containing high enriched uranium in aluminum clad. On the outside of the fuel elements (FE) are two concentric neutron absorbing control elements (CE), a large beryllium reflector, and light water. A mockup of the HFIR is shown in Fig. 1.

Each CE is composed of multiple regions of various neutron absorbing characteristics: a white region (Al) has low absorbing capabilities, a grey region (Ta-Al) has moderate absorbing capabilities, and a black region (Eu_2O_3-Al) has high absorbing capabilities. The control cylinder is used for regulation, and the safety plates are used for both regulation and safety. The beginning-of-cycle (BOC) and end-of-cycle (EOC) CE positions are illustrated in Fig. 2.

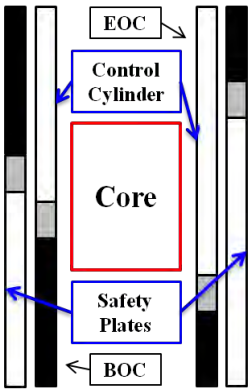

Figure 2. BOC and EOC CE configurations.

1.2 Reactor Physics Definitions

A macroscopic neutron cross section (Σ cm^{-1}) is the measure of the probability of a neutron-induced reaction (i.e., absorption, fission, etc.). Neutron flux (ϕ neutrons/cm^2-s) is a measure of the number of neutrons passing through a unit area perpendicular to the neutron stream per unit time. The effective multiplication factor (k_{eff}) is the ratio of the number of neutrons in one generation to the previous generation or, equivalently, the ratio of the neutron production rate to the destruction rate (absorptions + leakage) (Eq. 1). Reactivity (ρ cents) is a measure of the deviation in k_{eff} due to some change in the system (frequently a change from criticality, i.e., $k_{eff} = 1$) (Eq. 2).

$$k_{eff} = \frac{\text{neutrons in generation i}}{\text{neutrons in generation i-1}} = \frac{P}{A+L} \quad \textbf{(1)}$$

$$\rho = \frac{k_{eff}-1}{k_{eff}} = 1 - \frac{1}{k_{eff}} \quad \textbf{(2)}$$

1.3 Descriptions of Transients Studied

When neutron absorbing materials are inserted or ejected, negative or positive reactivity, respectively, is introduced, which perturbs both the power magnitude and shape. The insertion of positive reactivity increases k_{eff}, and thus, the production rate becomes greater than the destruction rate. This perturbation in power has the potential of engaging the safety system and causing unplanned shutdowns.

A control cylinder ejection transient could be initiated if the drive gear system fails, which would cause the control cylinder to move downward and away from the core at a velocity of about 1.68 cm/s. Following a 5 MW increase in power and a subsequent 10 ms delay time, the safety plates will insert according to Eq. 3.

$$\frac{d^2\Delta z}{dt^2} = \begin{cases} 4(g) - 19.7(\Delta z)(g) & for\ \Delta z \le 0.15\ m \\ g & for\ \Delta z > 0.15\ m \end{cases}$$

g is the acceleration due to gravity **(3)**

A second example of a reactivity-induced perturbation is the ejection of a "black rabbit" from the hydraulic tube located in the FT. Rabbits designated as "black" contain strong neutron absorbing materials. The Department of Energy/Office of Nuclear Energy Fuel Cycle Research and Development Program has requested HFIR assistance in irradiating nuclear fuel samples to study their temperature- and irradiation-dependent properties [2]. These fuel samples will be shielded by Gd to maximize the fast-to-thermal neutron flux ratio and to keep the heat generation rates within safety limits.

Experiments are being performed with representative rabbits to determine the maximum worth and corresponding axial positions in the FT from which these rabbits can be ejected from without causing a reactor shutdown due to an induced power perturbation. During these ejections, a black rabbit (L = 6.4 cm, r = 0.55 cm) containing a Gd rod (L = 2.5–4 cm, r = 0.33 cm) is ejected from the reactor midplane in the upward direction. Four aluminum rabbits (low absorbing) above and below the black rabbit are ejected all together and are replaced with water.

2. Use of COMSOL Multiphysics

COMSOL version 4.2 [3] was utilized for the simulations described herein. The time-dependent coefficient form partial differential equation (PDE) as solved by COMSOL is shown in Eq. 4. The basic nuclear data needed to solve the ST and PK equations were derived from NEWT [4], a steady-state, 2-D neutron transport (discrete ordinates) code in the SCALE v6 code package [5], and MCNP5 [6], a 3-D, Monte-Carlo-theory-based neutron transport code.

$$e_a \frac{\partial^2 u}{\partial t^2} + d_a \frac{\partial u}{\partial t} + \nabla \cdot (-c\nabla u - \alpha u + \gamma) + \beta \cdot \nabla u + au = f \quad \textbf{(4)}$$

In Eq. 4, u is the dependent variable, e_a is the mass coefficient, d_a is the damping/mass coefficient, c is the diffusion coefficient, α is the conservative flux convection coefficient, γ is the conservative flux source term, β is the convection coefficient, α is the conservative flux convection coefficient, and f is the source term.

2.1 Space-Time Kinetics

The HFIR assembly consists of multiple regions encompassing each other in a cylindrical geometry, which was modeled in COMSOL using 2-D axisymmetric geometry (r, z). A screenshot of the HFIR model is shown in Fig. 3

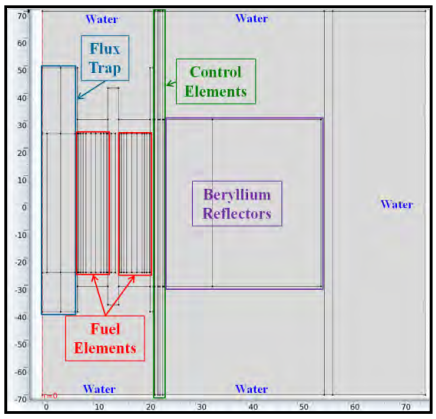

Figure 3. As-modeled HFIR geometry (cm).

with the pertinent regions outlined. The nuclear data for each of these regions were defined as local, domain-dependent variables.

2.1.1 Equation-based Modeling

Three studies are performed in sequential order to solve the three-energy-group (g=1:3) neutron diffusion equations (Eq. 5) and the six-group (i=1:6) delayed neutron precursor (DNP) equations (Eq. 6) with COMSOL's PDE application mode (delayed neutrons arise from the decay of fission products). The eigenvalue solver is used to calculate the static neutron flux distribution. However, the amplitude of the flux is internally normalized; thus, a stationary calculation must be carried out to normalize the fluxes to the desired initial power level. The stationary solution is then used as the initial conditions for the time-dependent calculation.

$$\frac{1}{v^g}\frac{\partial \phi^g}{\partial t} - \nabla \cdot D^g \nabla \phi^g + \left[\Sigma_a^g + \sum_{g'=1,\neq g}^{3} \Sigma_s^{g\rightarrow g'}\right]\phi^g = \sum_{g'=1,\neq g}^{3} \Sigma^{g'\rightarrow g}\phi^{g'} + (1-\beta_{eff})\chi_p^g \sum_{g'=1}^{3} \upsilon\Sigma_f^{g'}\phi^{g'} + \sum_{i=1}^{6} \chi_i^g \lambda_i C_i \quad \textbf{(5)}$$

$$\frac{\partial C_i}{\partial t} + \lambda_i C_i = \beta_i \sum_{g=1}^{3} \upsilon\Sigma_f^g \phi^g \quad \textbf{(6)}$$

The left- and right-hand-sides of Eqs. 5 and 6 define the loss and production mechanisms, respectively, and v is the average neutron speed, D is the diffusion coefficient, Σ_a is the absorption cross section, $\Sigma_s^{g\rightarrow g'}$ is the scattering cross section from g to g', $\nu\Sigma_f$ is the average number of neutrons emitted per fission times the fission cross section, β_i is the fraction of all fission neutrons emitted by DNPs in the i^{th} group, β_{eff} is the total delayed neutron fraction (sum of β_i's), C_i is the DNP concentration, λ_i is the decay constant, χ_p^g is the fraction of prompt neutrons born into g, and χ_i^g is the fraction of delayed neutrons from DNP group i born into g.

For the eigenvalue problem, the time-derivative terms (i.e., $\partial/\partial t$) are replaced by an eigenvalue term ($\lambda - \lambda_o$). Here, λ and λ_o are the eigenvalue (not k_{eff}) and the eigenvalue linearization point, respectively. For these studies, λ_o is set to zero and a λ value of zero is desired, which shows that neutron production is equal to neutron destruction (steady-state, 1st of the 3 studies). The max normalization method was used, which scales the dependent variables between zero and unity.

The eigenvalue solution is used as a sophisticated starting guess to the nonlinear stationary problem. The convergence rate of nonlinear stationary problems is strongly dependent on the starting guess, and thus, the solution converges faster if the initial guess is close to the solution.

In order to solve for k_{eff}, the eigenvalue problem is recast as a nonlinear stationary problem by applying a normalization constraint on the solution and by replacing the $\nu\Sigma_f$ terms in Eqs. 5 and 6 with $\nu\Sigma_f/k_{eff}$. For these analyses, it is assumed that power is only produced via neutron fission reactions, and since power is being studied, the neutron fluxes are normalized to the initial, steady-state power. The constraint shown in Eq. 7 was defined as an ODE in the Global Equations edit field. The notation is the same as before with the addition of the initial power (P watts) and the recoverable energy from fission ($\kappa \approx 3.2\text{x}10^{-11}$ J/fission).

$$k_{eff}: \left(\iiint \sum_{g=1}^{3} \kappa\Sigma_f^g \phi^g dV\right) - P_{initial} = 0 \quad \textbf{(7)}$$

The stationary solution is used as the initial conditions for the transient problem. During the transient calculations, reactivity-induced perturbations were simulated by moving the appropriate domains (i.e., CEs and/or stack of rabbits). Two methods can be used in COMSOL to simulate these movements: using the built-in Moving Mesh (ALE) module or defining time- and spatially-dependent properties. Since the

ALE module increases the number of degrees-of-freedom (DOF) and the moving domains are very long and thin, time- and axially-dependent properties were defined.

Rather than modeling the geometry of each CE as three separate cylinders (a white, grey, and black region), each with their own set of properties, the geometry of each CE was defined as one single cylinder. The z-coordinates corresponding to the grey/white and grey/black interfaces were described as time-dependent global variables and as functions of velocity, acceleration, ODE variables, etc. Then, "if" statements were used to describe the axially-dependent properties between these interfaces and the axial boundaries. A similar methodology was used for the rabbit ejection analysis, but the hydraulic tube was modeled as 6 different regions rather than 3. A smoothed Heaviside function [flc2hs(z-z_2,scale)] with a continuous second derivative was used to smooth the transition from heavy absorbers to low absorbers in the moving domains.

2.1.2 Boundary Conditions

The same boundary conditions (BC) were used for all three studies. For the neutron diffusion physics, a symmetry BC was used at the core centerline (r = 0), continuity boundary conditions were used at the interior domain interfaces, and vacuum BCs were used at the three outer pool surfaces (top, bottom, and outer radial). A vacuum BC uses the neutron flux slope at the boundary to extrapolate the flux outside of the physical boundary a distance d=2.1312D beyond the boundary, where the flux is assumed zero and D is the diffusion coefficient (Eq. 8). The DNP equations are distributed ODEs because they have no spatial derivatives. Therefore, zero flux BCs were applied to the outer edges of the fuel.

$$\phi_{\text{boundary}} = (-2.1312)(\text{D})|\nabla\phi|_{\text{boundary}} \quad \textbf{(8)}$$

2.2 Point Kinetics

Although increasing computational power and advances in simulation tools support the application of ST calculations for more comprehensive analyses, PK will continue to be utilized in the future because of short solution times and the results are usually conservative as compared to reality (PK methods over-estimate the impact of perturbations). Point kinetics equations with six DNP groups were also used in this work. The PK equations (7 ODEs for these studies) were coded into the Global Equations edit field (ODE solver).

The PK equations are derived from the reactor-averaged, time-dependent neutron balance (Eq. 9) and DNP balance (Eq. 10) equations.

$$\frac{d\langle n\rangle}{dt} = \left(1-\beta_{eff}\right)\langle \nu\Sigma_f,\phi\rangle - \langle\vec{\nabla}\cdot\vec{\mathrm{J}}\rangle - \langle\Sigma_a,\phi\rangle + \sum_{i=1}^{6}\lambda_i C_i(t) \quad \textbf{(9)}$$

$$\frac{dC_i(t)}{dt} = \beta_i\langle\nu\Sigma_f,\phi\rangle - \lambda_i C_i(t) \quad \textbf{(10)}$$

The notation is the same as before with the addition of n, the neutron density, and $\vec{\nabla}\cdot\vec{\mathrm{J}}$, the net leakage of neutrons. Point kinetics assumes that the time-dependent neutron flux is separable from the energy and space domains. Thus, the flux is written as a product of a shape function and an amplitude function. The leakage and absorption terms in Eq. 9 can be removed by introducing k_{eff} as defined previously. Reactivity as previously described is then substituted for k_{eff}; thus, yielding Eq. 11.

$$\frac{d\langle n\rangle}{dt} = \langle\nu\Sigma_f,\phi\rangle\left(\rho-\beta_{eff}\right) + \sum_{i=1}^{6}\lambda_i C_i(t) \quad \textbf{(11)}$$

Next, a proportionality constant is used to relate the number of neutrons to the fission rate. The mean generation time is defined in Eq. 12.

$$\Lambda = \frac{\langle n\rangle}{\langle\nu\Sigma_f,\phi\rangle} = \frac{\langle 1/\mathrm{v},\phi\rangle/\langle\phi\rangle}{\langle\nu\Sigma_f,\phi\rangle/\langle\phi\rangle} = \left(\bar{\mathrm{v}}\overline{\nu\Sigma_f}\right)^{-1} \quad \textbf{(12)}$$

The PK equations are formed by inserting Eq. 12 into Eqs. 10 and 11. The neutron density (n) can be replaced with neutron flux (ϕ) or power (P) since they are all proportional to each other.

$$\frac{dn(t)}{dt} = n(t)\left[\frac{\rho(t)-\beta_{eff}}{\Lambda}\right] + \sum_{i=1}^{6}\lambda_i C_i(t) \quad \textbf{(13)}$$

$$\frac{dC_i(t)}{dt} = n(t)\left(\frac{\beta_i}{\Lambda}\right) + \lambda_i C_i(t) \quad \textbf{(14)}$$

The stationary model (2nd of the 3 studies) was utilized to determine the worth of the control cylinder during ejection and the worth of the

safety plates during insertion. Static cases were executed to compute time-dependent effective multiplication factors, which were converted into reactivity using β_{eff} = 0.00762. The as-modeled reactivity worth of the control cylinder was determined to be about 85 cents/s or about 51 cents/cm if being ejected at 1.68 cm/s.

The safety plates' worth was calculated by positioning both control elements at multiple time-dependent positions, calculating the worth of the configuration with respect to the initial position, and then subtracting the reactivity worth of the control cylinder. It was determined that the worth of the safety plates was not linear with respect to time because they are worth more initially when the grey and black regions are adjacent to the control cylinder's white region and are worth less when the black region of the safety plates is next to the control cylinder's black region. The initial and final reactivity worth of the safety plates was determined to be about -55 and -17 cents/cm, respectively.

For the PK simulations, the control cylinder's movement was specified as 1.68 cm/s and the worth was defined as 51 cents/s. The movement of the safety plates defined by Eq. 3 was specified following a 10 ms response time after the scram set point was reached. The safety plates worth/cm vs. position curve was inserted into an interpolation table and the worth of the safety plates was calculated based on its position.

For the rabbit ejection PK studies, the axial flux shape in the hydraulic tube was used to weight the importance of each rabbit based on their axial location in the stack of 9 rabbits. The reactivity worth of the rabbits at the core horizontal midplane with respect to a water filled hydraulic tube was determined [7 and 8].

Then, these worths were normalized to the axially-dependent weighting factor. The relative neutron flux at the horizontal midplane is assumed to be unity and the relative flux shape is described by a cosine function such that the relative flux as a function of axial position is described by Eq. 15 [9]. The importance weighting factor is calculated by taking the square of the relative flux. The relative flux is shown pictorially in Fig. 4.

$$\phi_{rel} = \cos\left[0.0423\left({}^{1}/_{cm}\right)z(cm)\right], \quad for -34.29 > z > 34.29\ cm$$
$$\phi_{rel} = 0,\ otherwise \qquad \textbf{(15)}$$

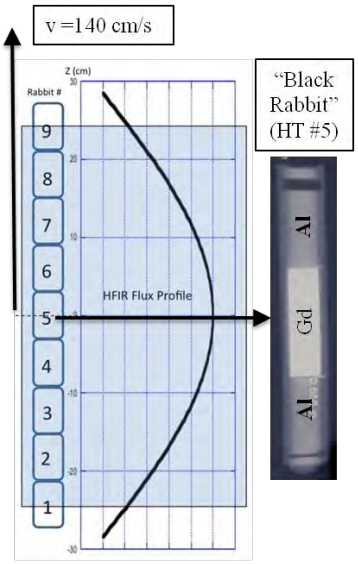

Figure 4. Rabbit configuration and flux profile.

The control cylinder's worth during the transient was defined by normalizing the measured control cylinder voltage data such that the initial worth was set to zero (prior to the ejection) and the final (negative) worth was set equal to the (positive) worth of the stack of rabbits with respect to a water filled hydraulic tube. The worth curve was described by an algebraic equation as a global definition.

3. Results of Simulations

For the ST eigenvalue and stationary simulations, the PARDISO direct solver was used. The MUMPS direct solver was used for the transient studies in order to utilize distributed parallel processing. One compute node containing 8 cores on two processors with 64 GB RAM was utilized for the eigenvalue and stationary studies while 3 of these compute nodes were used for the transient studies. For the ST simulations, approximately 75 - 150 thousand mesh elements were used to discretize the geometry and 1 - 2 million DOF were solved.

The static, BOC three-group [fast (0.1 MeV ≤ E_n ≤ 20 MeV), epithermal (0.625 eV ≤ E_n ≤ 0.1 MeV), and thermal (10 μeV≤ E_n ≤ 0.625 eV)] neutron flux distributions are shown in Fig. 5. As viewed in this figure, fast neutrons are born in the fuel regions and leak into the water and beryllium regions where they are moderated to lower energies.

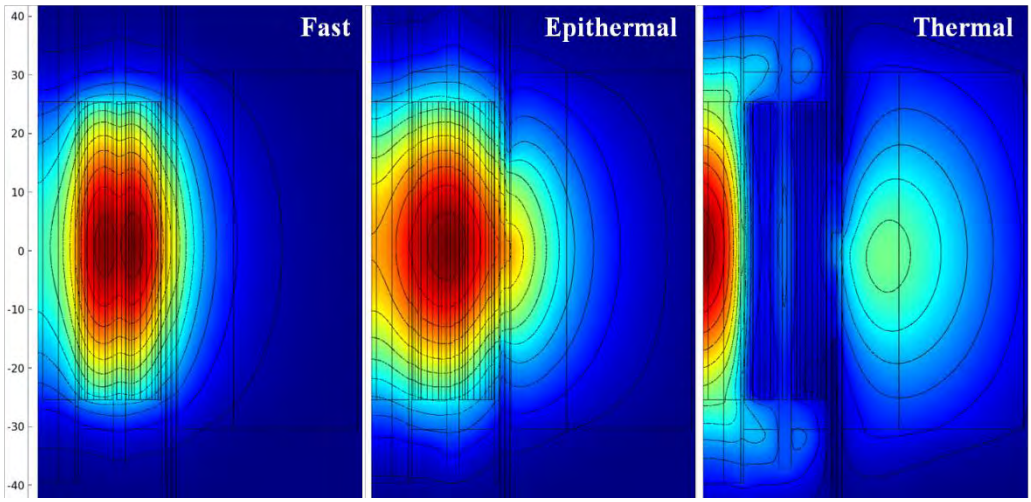

Figure 5. BOC three-group neutron flux distributions (dimensions in cm).

The initial power for the control cylinder ejection is 1 kW, which approximates a zero power condition. Low power transients are of concern because more reactivity is added prior to a scram being initiated. Thus, the lower the initial power is, the greater the peak power to initial power ratio will be.

The scram set point of 5.001 MW was reached about 1.365 seconds into the transient, and the safety plates began moving 10 ms later. The max power (10.63 MW) was achieved 1.39 seconds into the transient. The control cylinder's and safety plates' grey/white region interface locations with respect to the midplane are shown with the power curve in Fig. 6. The power distribution prior to ejection, at the time of peak power, and 1.7 seconds after the transient was initiated are shown in Fig. 7.

The time-dependent worth curves described previously were defined in the PARET ([10] and [11]) and COMSOL PK inputs. The PARET code is maintained by Argonne National Laboratory and couples PK, heat transfer (1-D), and hydrodynamics (1-D) to study nondestructive transients in light water research reactors with pin- or plate-type fuel elements.

As viewed in Fig. 6, the max power calculated with PARET after setting all the feedback coefficients (fuel temperature, moderator temperature, and void) equal to zero [P(1.39 s) = 10.18 MW] is in good agreement with the ST COMSOL model. The max power calculated by the PARET model with feedback [P(1.40 s) = 9.70 MW] is slightly less than the models not employing feedback because HFIR has negative moderator and Doppler temperature coefficients. Thus, negative reactivity is introduced when the fuel and moderator temperatures increase.

The max power calculated in the COMSOL PK model (P = 10.10 MW) occurred 1.43 seconds after the transient was initiated. The 0.04 second difference between the COMSOL ST and PK models is likely caused by the PK model assuming no spatial variation in the power. The PARET code is in better agreement with the ST results because the PARET model divides the reactor into 323 zones and each zone has a different power generation.

At this time, additional effort is required to implement the ST black rabbit ejection simulation, but PK solutions are provided for this transient. The results from one of the BOC 434 (February, 2011) low power 3.81 cm long Gd rod and full power 2.54 cm long Gd rod ejections are shown in Fig. 8. The PK results agree well with the measured data.

All cases were analyzed with a 140 cm/s ejection velocity and the peak transient power occurred about 0.20 seconds after the ejection was initiated. A 2.2 MW increase in power was calculated for the 2.54 cm long Gd rod ejection at an initial reactor power of 84.6 MW (2.6 % increase). At an initial power of about 12 MW, a 3.81 cm long Gd rod ejection caused the power to increase about 0.5 MW (4.2 % increase).

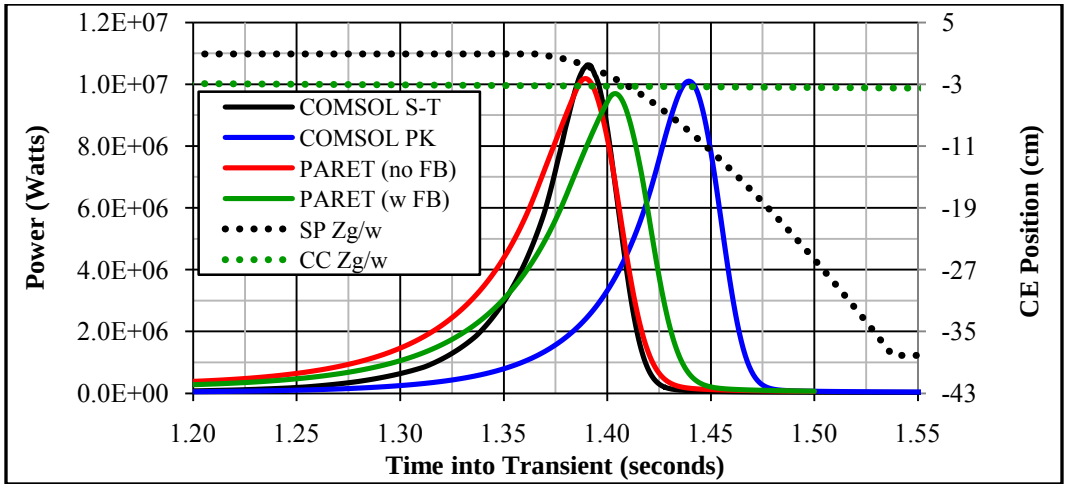

Figure 6. Control cylinder ejection transient power and control element movement curves.

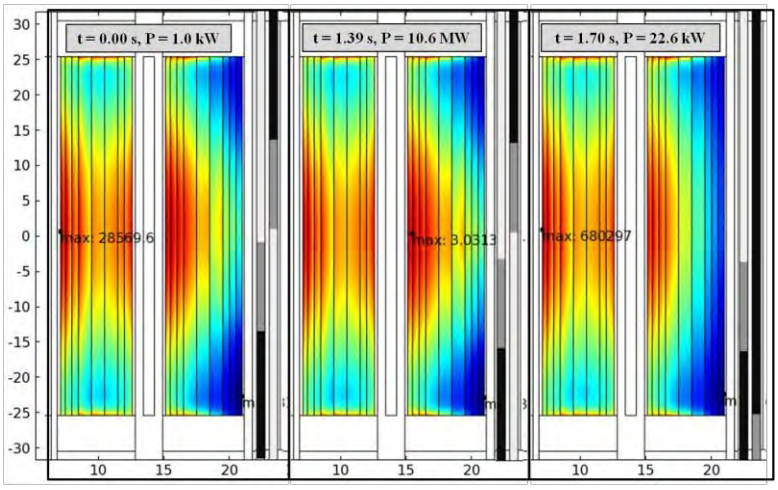

Figure 7. Power distribution during control cylinder ejection transient (dimensions in cm).

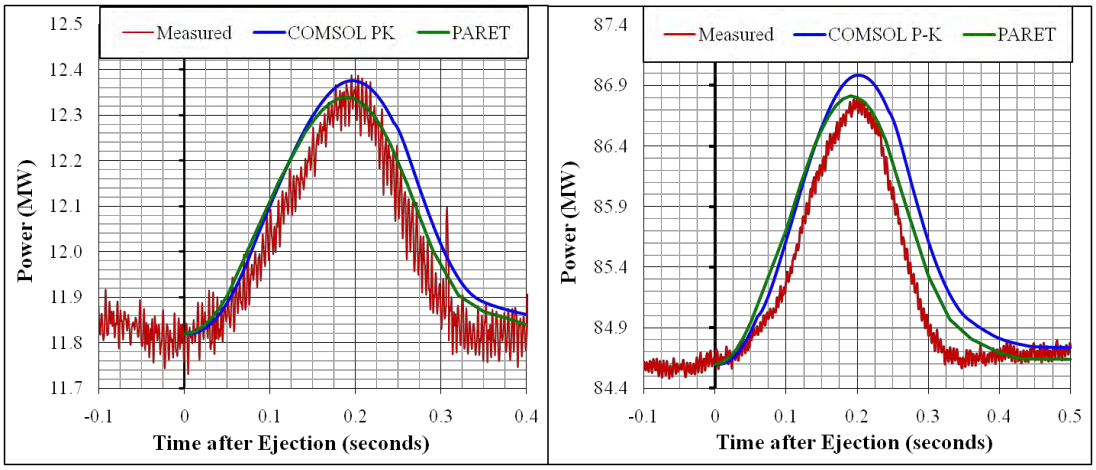

Figure 8. BOC rabbit ejection power curves (left: low power 3.81 cm Gd, right: full power 2.54 cm Gd).

4. Conclusions

Space-time and point kinetics methodologies were developed in COMSOL version 4.2 for predicting the dynamic behavior of the HFIR core in response to reactivity-induced perturbations. The space-time simulations utilized the PDE coefficient application mode and 2-D axisymmetric geometry to solve the three-group neutron diffusion equations. The basic nuclear data were calculated with the NEWT and MCNP5 neutron transport codes.

The space-time models developed in this research only considered the neutronics aspect of kinetics, and therefore, do not include fluid flow or heat transfer physics or reactivity feedback. Thermal hydraulic and structural models are currently being developed at HFIR and variations of these models are expected to eventually be merged together to form a comprehensive multiphysics methodology for studying the dynamic behavior of the HFIR core during reactivity-induced perturbations.

The COMSOL ODE application mode was utilized to solve the point kinetics equations. Global equations and algebraic equations were developed to describe the motion and reactivity worth of the control elements and stack of rabbits as a function of time. In conclusion, the point kinetics methodologies employed here are sufficient for these types of analyses as long as local information is not desired.

5. References

1. D. Chandler, R. T. Primm, III, G. I. Maldonado, and J. D. Freels, *Neutronics Modeling of the High Flux Isotope Reactor using COMSOL*, Annals of Nuclear Energy, doi: 10.1016/j.anucene.2011.06.002 (2011)

2. R. W. Hobbs and B. F. Siefken, *High Flux Isotope Reactor (HFIR) Rabbit Ejection Tests*, ORNL/HFIR/SBS/2010-01/R0, Oak Ridge National Laboratory, internal publication at the Oak Ridge National Laboratory, contact Research Reactors Division for distribution (2011)

3. COMSOL, Inc., *COMSOL Multiphysics User's Guide*, Version 4.2, Burlington, MA (2011)

4. M. D. DeHart, *NEWT: A New Transport Algorithm for Two-Dimensional Discrete Ordinates Analysis in Non-Orthogonal Geometries*, ORNL/TM-2005/39, Version 6, Vol. II, Oak Ridge National Laboratory (2009)

5. *SCALE: A Modular Code system for Performing Standardized Computer Analyses for Licensing Evaluations*, ORNL/TM-2005/39, Version 6, Vols. I - III, Oak Ridge National Laboratory (2009)

6. X-5 Monte Carlo Team, *MCNP—A General Monte Carlo N-Particle Transport Code*, Version 5, LA-CP-03-0245, Los Alamos National Laboratory (2003)

7. R. J. Ellis, *Heat Generation and Neutronics Calculations in Support of Black Rabbit Experiments in HFIR*, C-HFIR-2010-011, internal, archived publication at the Oak Ridge National Laboratory, contact Research Reactors Division for distribution (2010)

8. R. W. Hobbs, *Reactivity Worth of Rabbits Containing Partial Length Gadolinium Rods or Sleeves*, C-HFIR-2011-007, internal, archived publication at the Oak Ridge National Laboratory, contact Research Reactors Division for distribution (2011)

9. Personal communication with R. W. Hobbs, Oak Ridge National Laboratory (2011)

10. A. P. Olson, *A Users Guide to the PARET/ANL V7.2 Code – Draft, Reduced Enrichment for Research and Test Reactor (RERTR) Program*, Argonne National Laboratory (2006)

11. C. G. Velit, R. T. Primm, III, and J. C. Gehin, *Partial Safety Analysis for a Reduced Uranium Enrichment Core for the High Flux Isotope Reactor*, ORNL/TM-2007/226, Oak Ridge National Laboratory (2009)

6. Acknowledgements

The studies documented in this paper were made possible by a research contract between the University of Tennessee Nuclear Engineering Department and the Research Reactors Division of the Oak Ridge National Laboratory. The authors would like to thank Mr. R. W. Hobbs (ORNL, Research Reactors Division) and the COMSOL technical support staff for their advice during the development of the models described in this paper.